# Superplasticity in a high-manganese (nickel free) stainless steel

**G. PIATTI, D. BOERMAN and H.A. WEIR, Materials Science Division, Ispra Establishment, Joint Research Centre, Commission of the European Communities, Ispra, Italy.**

**Abstract**

*Mechanical (tensile tests) and microstructural (optical and scanning electron microscopy) investigations have been performed on a heavily cold-rolled nickel-free stainless steel plate having a nominal (weight percent) composition: 14 Cr-20 Mn-balance Fe. Preliminary results, showing superplastic behaviour exhibited by this high-manganese stainless steel, when deformed in the temperature range 20 to 900°C and at a low initial strain rate ($\dot{\varepsilon}_i \leq 1.5 \times 10^{-3} s^{-1}$), are reported and discussed.*

**Riassunto**

**Comportamento superplastico in un acciaio inossidabile ad elevato tenore di manganese**

Sono state eseguite prove meccaniche (deformazione a trazione) ed esami microstrutturali (microscopia ottica ed elettronica a scansione) su un acciaio inossidabile privo di nickel, laminato a temperatura ambiente e di composizione nominale in peso: 14 Cr-20 Mn.

Nel presente lavoro vengono presentati e discussi i risultati ottenuti, i quali mettono in evidenza come questo acciaio ad elevato tenore di manganese presenti un comportamento superplastico a basse velocità di deformazione ($\dot{\varepsilon}_i \leq 1{,}5 \times 10^{-3} s^{-1}$) nell'intervallo di temperatura 20 - 900°C.

## Introduction

Superplasticity was reported for chromium-nickel stainless steels having a composition very near the nominal (weight percent) composition: 26 Cr-6.5 Ni-balance Fe (1-4) and also for stainless steels containing aluminium and manganese substituted for chromium and nickel respectively (5). This paper also discusses the subject of superplastic flow in stainless steels. More precisely, the authors present preliminary results concerning the phenomenon of superplasticity in a particular class of stainless steels, the iron-chromium-manganese (nickel-free) alloys. These materials have recently been investigated for their potential application in thermonuclear fusion reactors (6-9) and superplasticity could be important in nuclear engineering (10).

## Material and experiment

The starting material was an experimental high-manganese stainless steel, AMCR 0035-Creusot-Loire. The composition of this steel is given in Table 1. This alloy, according to the Fe-Cr-Mn phase diagram, recently reviewed by Charles (11), is characterized by a duplex $\gamma$ – austenite + $\alpha$ – ferrite structure. In fact, the microstructure (Fig. 1a) consists of about 15% by volume of $\alpha$ – ferrite second phase dispersed in a $\gamma$ – austenite matrix, enriched with chromium but impoverished in manganese with respect to the austenite (Table 1).

The steel, supplied in the form of mill-annealed plate, was heavily cold rolled (reduction in thickness above 70%) into 1 mm thick sheets, with the effect of breaking up the initial grains and producing an intimate mixture of $\alpha$ and $\gamma$ phases (Fig. 1b). No annealing was used after the rolling process in the two-phase field and before the tensile tests, because the static recrystallization, which occurred during heating plus the 30 min. soaking time necessary to ensure a uniform test temperature, was achieved in the tensile specimens before the start of deformation, was generally enough to produce the ($\gamma + \alpha$) microduplex structure (Fig. 1c) necessary for superplastic behaviour,

## TABLE 1 - Alloy and structural phases composition.

| Element | Cr | Mn | Si | C | N | S | P | Ni | Mo | Cu | Al | Pb | B | Fe |
|---|---|---|---|---|---|---|---|---|---|---|---|---|---|---|
| Alloy* (AMCR 0035 Creusot-Loire) | 14.09 | 19.88 | 0.63 | 0.029 | 0.048 | 0.006 | 0.018 | 0.265 | <0.06 | <0.05 | <0.004 | 1 ppm | 28 ppm | rest |
| $\gamma$ – phase** | 14.07 | 19.95 | 0.96 | — | — | — | — | 0.21 | — | — | — | — | — | — |
| $\alpha$ – phase** | 18.91 | 17.95 | 0.96 | — | — | — | — | 0.28 | — | — | — | — | — | — |

* Average values determined in percent by weight by chemical analysis.
** Average values determined in percent by weight by SEM/EDS microanalysis.

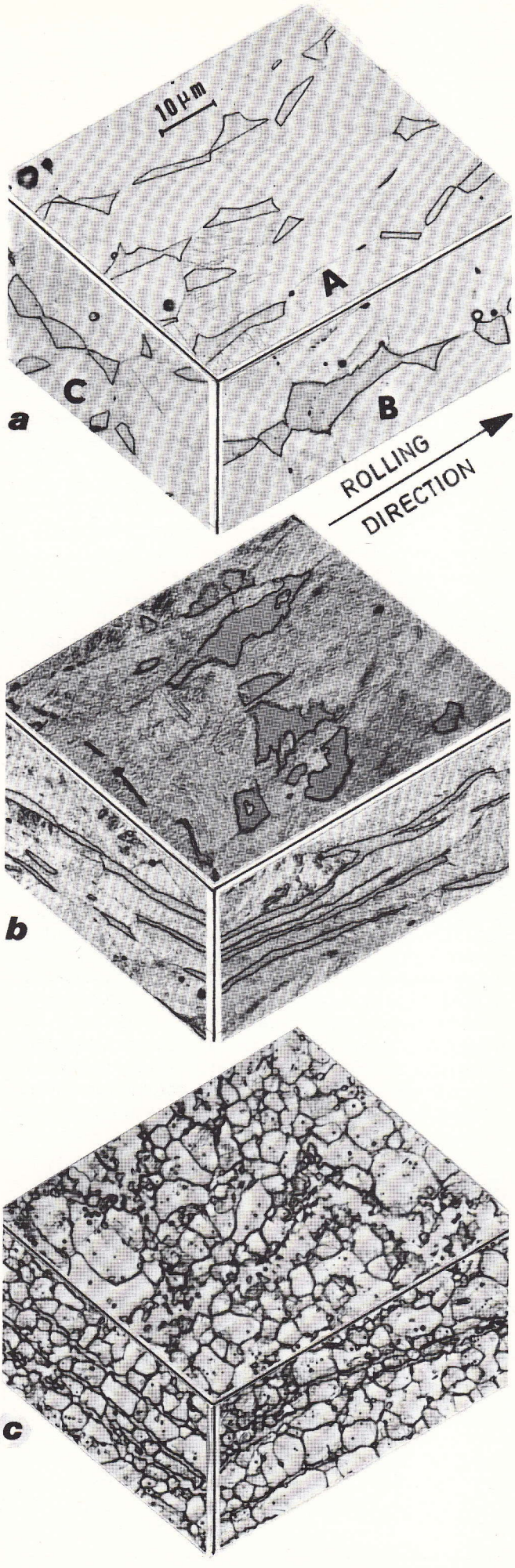


Fig. 1 - Composite microstructure of the cold-rolled 14 Cr-20 Mn stainless steel investigated: a) in as received (mill-annealed) conditions; b) after cold-rolling; c) after cold-rolling and heating plus soaking time at 875°C prior to start of deformation:
A = large longitudinal (to rolling direction) section
B = narrow longitudinal section
C = transverse section
(optical micrographs at the same magnification).

according to the design rules recently reviewed by Stowell (1). Moreover, the specimens, which were not recrystallized during the heating plus soaking treatment, recrystallized progressively during the early part of subsequent tensile straining at high temperature.
In fact, manganese addition to Fe-Cr alloys lowers the stacking fault energy (11) and, in the present case, was sufficient for dynamic recrystallization to occur. The tensile tests were run on an Instron electro-mechanical machine, in vacuum, over wide ranges of temperature (700, 750, 800, 825, 850, 875, 900, 950 and 1000°C) and strain rates ($1.04 \times 10^{-4}$, $2.08 \times 10^{-4}$, $4.16 \times 10^{-4}$, $1.04 \times 10^{-3}$, $1.04 \times 10^{-2}$ and $1.04 \times 10^{-1} s^{-1}$) using flat specimens (8 mm gauge length and 2 mm gauge width) stamped from sheets with their axes parallel to the rolling direction.

## Results

Fig. 2 shows the influence of strain rate on the maximum engineering stress at 850°C. A regression analysis indicated that the experimental points should be fitted to two straight lines with high correlation coefficients. Then two conventional stages according to the literature (12-13), were delineated: region II at low strain rates ($\dot{\varepsilon}_i \leq 1.5 \times 10^{-3} s^{-1}$) where the strain-rate sensitivity index, m = 0.364 (determined from the slope of the line), is >0.30 (superplasticity regime) and III at intermediate and high strain rates ($\dot{\varepsilon}_i > 1.5 \times 10^{-3} s^{-1}$) where, m = 0.196, is <0.30 (conventional plasticity regime). There was no evidence at low strain rates of a conventional region I characterized by m >0.30. Although most superplastic systems show the well known three-stage relationship between log stress and log strain rate, there is also a number of examples where there is no region I (14-16).

Fig. 2 - The stress vs. strain rate relation for the cold-rolled 14 Cr-20 Mn stainless steel deformed at 850°C.

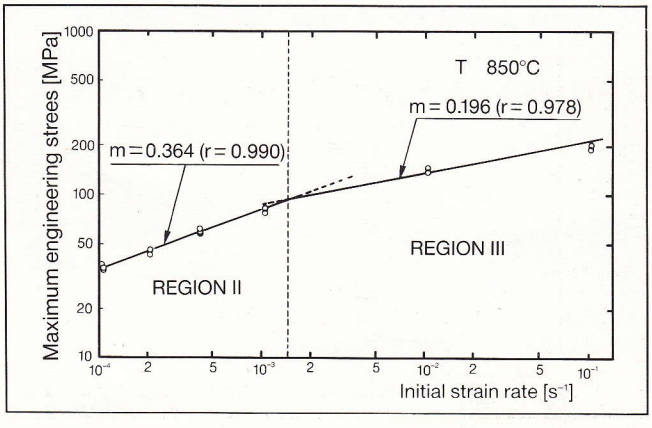

The relationship between flow stress and strain rate was strongly influenced by the temperature, as shown in Table 2, where the m values are listed for four selected temperatures. The strain rate sensitivity index increased with the temperature to a maximum at 850°C (m = 0.364, see also Fig. 2). Above this temperature, the change in phase proportion (reduction in α – phase volume fraction) leads to a significant grain coarsening, the m value decreases and, at 1000°C, the highest temperature investigated, $m = 0.176 < 0.30$ and superplasticity is lost. A strict correlation exists between the strain-rate sensitivity index and the ductility, which are together reliable indicators of the superplastic potential. Elongations at fracture ($e_f$) greater than 200% are evident (Fig. 3) in superplastic region II ($\dot{\varepsilon}_i = 1.04 \times 10^{-4}$ and $1.04 \times 10^{-3} s^{-1}$) with peaks in ductility at 850°C (maximum value 395%),

## TABLE 2 - Effect of temperature on m values*

| Temperature (°C) | m (Region II) | m (Region III) |
|---|---|---|
| 825 | 0.352 (r = 0.988) | 0.190 (r = 0.986) |
| 850 | 0.364 (r = 0.990) | 0.196 (r = 0.978) |
| 875 | 0.316 (r = 0.984) | 0.184 (r = 0.996) |
| 1000 | — | 0.176 (r = 0.941) |

* Determined from the log-log plots of max. engineering stress vs. initial strain rate.

Fig. 3 - Variation of elongation to fracture with temperature for the cold-rolled 14 Cr-20 Mn stainless steel deformed at four different initial strain rates.

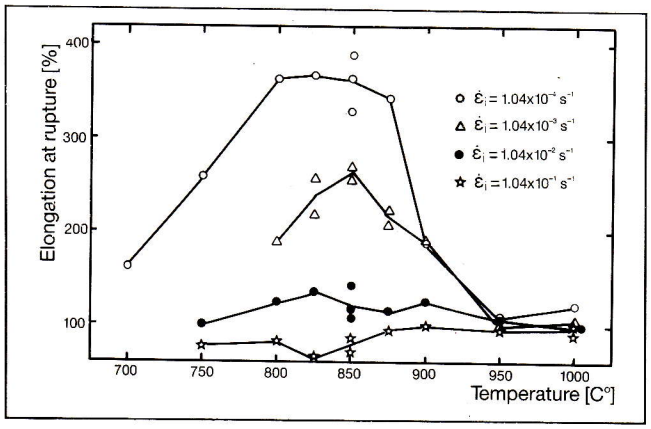


whereas in region III ($\dot{\varepsilon}_i = 1.04 \times 10^{-2}$ and $1.04 \times 10^{-1} s^{-1}$) the ductility drops below 150%. Strain effects are also present.

Fig. 4 shows a representative set of the true stress (σ) – true strain (ε) curves calculated assuming constant volume of the specimen during tensile deformation, from the Instron load v. elongation results, obtained at different initial strain rates ($\dot{\varepsilon}_i$) and at 850°C. At all the strain rates investigated there was an immediate strain hardening, followed at intermediate and low strain rates ($\dot{\varepsilon}_i < 1.04 \times 10^{-3} s^{-1}$) by a steady-state superplastic flow in which the stress was essentially strain independent. There was then instability in flow, during the early part of deformation. On the other hand, at the highest strain rate investigated ($\dot{\varepsilon}_i \geq 1.04 \times 10^{-3} s^{-1}$) the behaviour tended to be more conventional (non-superplastic), as shown by the decrease in stress as a result of necking, due to relatively low values of strain-rate sensitivity with high rates. The strain hardening can be attributed to concurrent grain coarsening. There are several similar cases in recent literature, where the connection between strain hardening and grain growth in superplastic behaviour is clearly established (16-21).

Internal changes produced during superplastic deformation were revealed by optical and scanning electron microscope (SEM) analysis. The α – banded morphology, present in the recrystallized conditions (Fig. 1c), was spheroidized to yield an almost equiaxed shape, principally during the early part of superplastic deformation. Limited γ – phase coarsening of the order of 85%, after about 400% deformation, was observed at 850°C, where the superplastic effect was at its maximum. These microstructural changes were strain enhanced, as evidenced in Table 3, which shows the values of the γ – mean grain sizes, obtained by a linear intercept method, as a function of the test parameters.

Fig. 4 - True stress - true strain curves at 850°C for the cold-rolled 14 Cr-20 Mn stainless steel deformed at different initial strain rates.

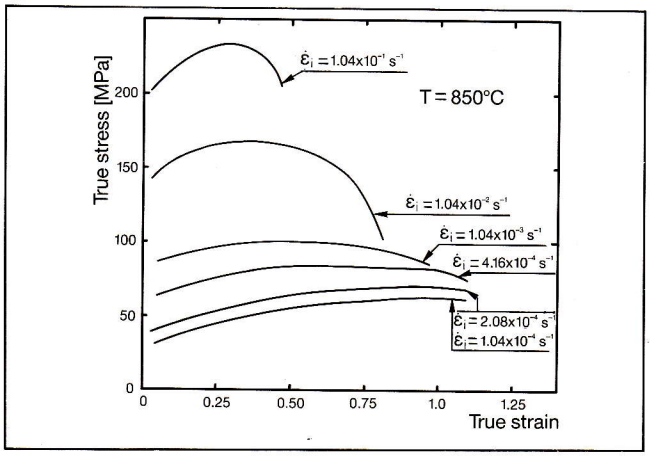

**TABLE 3 - Changes in γ-grain size ($\bar{L}$) of the cold-rolled 14 Cr-20 Mn stainless steel due to superplastic deformation.**

| Initial microstructure | Experimental conditions | | | Microstructure after static coarsening (specimen grip region) | Microstructure after dynamic coarsening (specimen rupture zone) |
|---|---|---|---|---|---|
| $\bar{L}$ [μm] | $\dot{\varepsilon}_i$ [$s^{-1}$] | T [°C] | $e_f$ [%] | $\bar{L}$ [μm] | $\bar{L}$ [μm] |
| 50 ± 5.0 | $1.04 \times 10^{-6}$ | 850 | 390 | 4.35 ± 0.60 | 6.34 ± 0.79 |
| (as supplied) | $2.08 \times 10^{-4}$ | 850 | 385 | 3.40 ± 0.36 | 5.76 ± 0.58 |
| 12.8 ± 10.2 | $4.16 \times 10^{-4}$ | 850 | 278 | 2.38 ± 0.31 | 4.22 ± 0.20 |
| (after cold-rolling) | $1.04 \times 10^{-3}$ | 850 | 270 | 2.09 ± 0.48 | 3.68 ± 0.38 |
| 3.44 ± 0.52 | $1.04 \times 10^{-2}$ | 850 | 142 | 1.24 ± 0.14 | 2.19 ± 0.12 |
| (after cold-rolling | $1.04 \times 10^{-1}$ | 850 | 84 | 1.30 ± 0.15 | 1.90 ± 0.21 |
| and soaking at 875°C) | $1.04 \times 10^{-3}$ | 800 | 189 | 1.80 ± 0.22 | 1.82 ± 0.25 |
| | $1.04 \times 10^{-3}$ | 825 | 217 | 1.13 ± 0.07 | 2.09 ± 0.25 |
| | $1.04 \times 10^{-3}$ | 850 | 270 | 2.09 ± 0.47 | 3.68 ± 0.38 |
| | $1.04 \times 10^{-3}$ | 875 | 223 | 3.52 ± 0.36 | 4.39 ± 0.56 |
| | $1.04 \times 10^{-3}$ | 900 | 190 | 7.93 ± 1.73 | 4.83 ± 1.08 |
| | $1.04 \times 10^{-3}$ | 950 | 101 | 15.68 ± 4.64 | 16.55 ± 5.00 |
| | $1.04 \times 10^{-3}$ | 1000 | 106 | 15.09 ± 2.23 | 19.20 ± 5.32 |

During deformation, cavities were formed, principally at the boundaries between γ – matrix grains and α – second phase particles. The volume cavities increased with increasing strain, with decreasing strain-rate and increasing temperature. Cavitation was found to have influenced the fracture behaviour.
Under the test conditions resulting in superplastic flow, fracture occurred by coalescence of grain-boundary cavities, and interlinkages were also found (Fig. 5).
As regards the external appearance of the deformed specimens, a considerably rumpled or granular surface was revealed by the SEM images. Fig 6 shows the surface appearance of specimens broken at 850°C and at strain rates in region II. Clumps of grains move relatively to each other, but there is little relative movement of grains within each clump. These features can be explained by the occurrence of grain-boundary sliding processes (12-13).

## Conclusions

a) Cold-rolled 14 Cr-20 Mn stainless steel exhibits a superplastic behaviour manifested by a high elongation at fracture ($e_f > 300\%$) and a high strain-rate sensitivity ($m > 0.30$) when deformed at elevated temperatures ($750 < T < 900$°C) and at low strain rates ($e_i \leq 1.5 \times 10^{-3} s^{-1}$).
b) Superplasticity in the alloy is accompanied by limited strain-enhanced grain growth and evident intergranular cavitation.


## Aknowledgements

The authors thank Miss T. Stoto for her contribution.


Fig. 5 - Ion etched longitudinal section of cold-rolled 14 Cr-20 Mn stainless steel deformed at 850°C at an initial strain rate of $2.08 \times 10^{-4} s^{-1}$ (total elongation 385%) (SEM image).

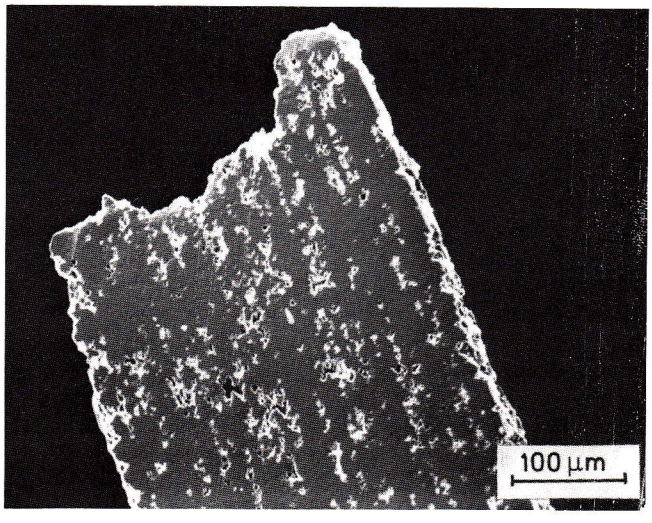

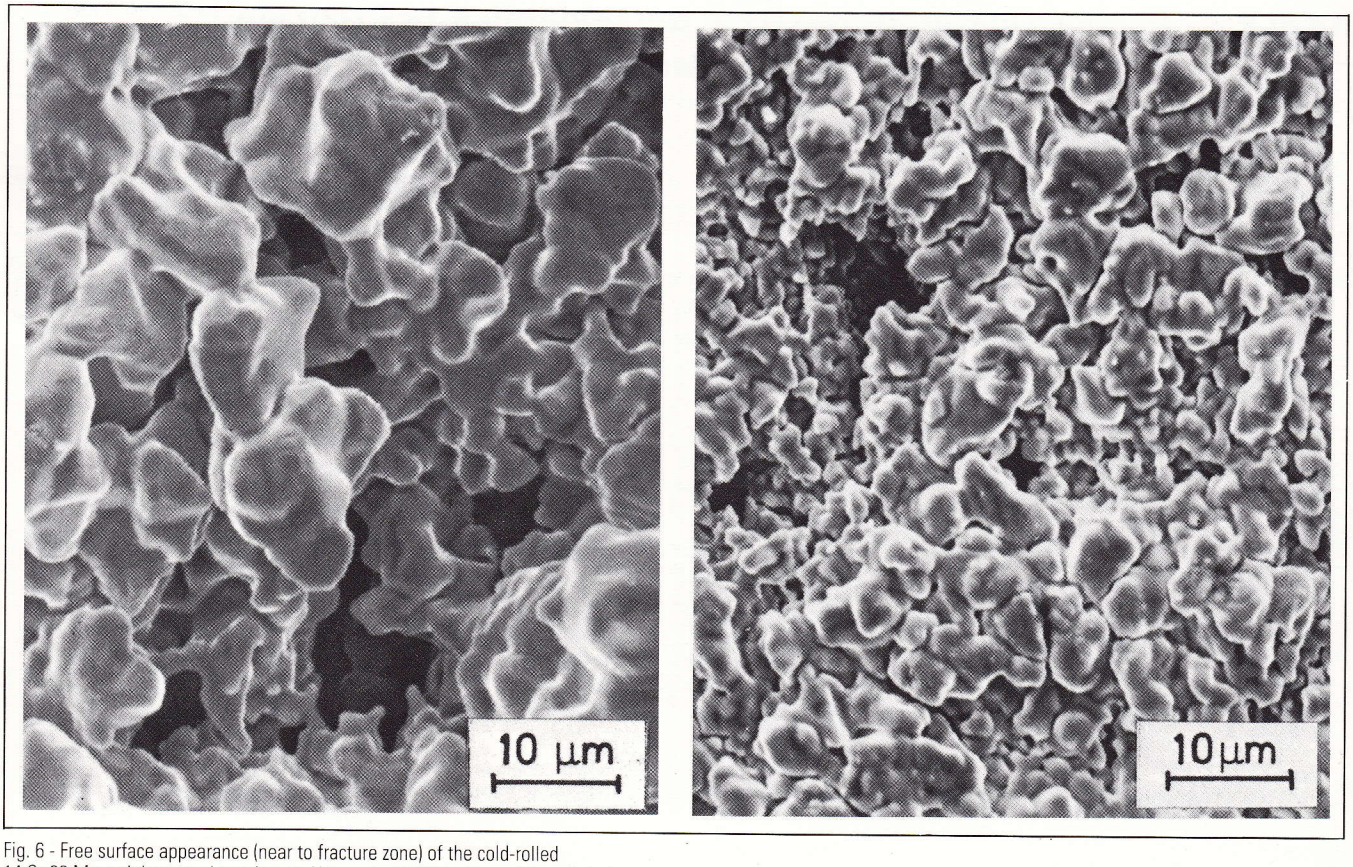


Fig. 6 - Free surface appearance (near to fracture zone) of the cold-rolled 14 Cr-20 Mn stainless steel specimens deformed at 850°C at two different strain rates:
a) $1.04 \times 10^{-4}$ and b) $1.04 \times 10^{-3} s^{-1}$ (SEM images).


*REFERENCES*

*(1) Stowell, M.J. In J.B. Bilbe-Sørensen et al. (Eds.), Proc.* **4th Int. Symp. Metallurgy and Material Science**, *Roskilde, Denmark, 1983, p. 119.*

*(2) Gibson, R.C., H.W. Hayden, and J.H. Brophy.* **Trans. ASM, 61** *(1968), 85.*

*(3) Smith, C.I., B. Norgate, and N. Ridley.* **Metal Sci., 10** *(1976), 182.*

*(4) Ward, D.M.* **Sheet Metal Ind., 59** *(1982), 28.*

*(5) Toscano, E.H.* **Scripta Met., 17** *(1983), 309.*

*(6) Fenici, P., D. Boerman, V. Coen, E. Lang, C. Ponti, and W. Schule.* **Nucl. Eng. Design-Fusion, 1** *(1984), 167.*

*(7) Piatti, G., S. Matteazzi, and G. Petrone.* **Nucl. Eng. Design-Fusion, 2** *(1985), 391.*

*(8) Piatti, G., and G. Musso. To be published in* **J. Mater. Sci.** *(1986).*

*(9) Snykers, M., and E. Ruedl.* **J. Nucl. Mater., 103 & 104** *(1981), 1075.*

*(10) Gittus, J.* **Res. Mechanica, 7** *(1983), 127.*

*(11) Charles, J. Thesis. Université Catholique de Louvain, Louvain-La-Neuve, Belgium, 1982.*

*(12) Edington, J.W., K.N. Melton, and C.P. Cutler.* **Progr. Mater. Sci., 21** *(1976), 61.*

*(13) Padmanabhan, K.A., and G.J. Davies.* **Superplasticity**. *Springer-Verlag, Berlin, 1980, p. 15.*

*(14) Rai, G., and N. Grant.* **Metal. Trans. 6A** *(1975), 385.*

*(15) Lam, S.T., A. Arieli, and A.K. Mukherjee.* **Mater. Sci. Eng., 40** *(1979), 73.*

*(16) Piatti, G.* **J. Mater. Sci., 18** *(1983), 2471.*

*(17) Kashyap, B.P., and A.J. Mukherjee. In R.C. Gifkins (Ed.), Proc.* **6th Int. Conf. on Strenth of Metals and Alloys**, *Melbourne. Pergamon Press, Oxford, 1982, p. 707.*

*(18) Suery, M., and B. Baudelet. In G. Bernasconi and G. Piatti (Eds.),* **Creep of Engineering Materials and Structures**. *Applied Science Ltd., London, 1979, p. 47.*

*(19) Livesey, D.W., and N.J. Ridley.* **J. Mater. Sci., 13** *(1978), 825.*

*(20) Watts, B.M., and M.J. Stowell. Ibid.,* **6** *(1971), 228.*

*(22) Piatti, G., and T. Stoto.* **J. Mater. Sci. Letters, 3** *(1984), 1020.*